SCUOLA DI INGEGNERIA INDUSTRIALE
E DELL'INFORMAZIONE

Executive Summary of the Thesis

Numerical modeling of REBCO Pancake Coils with PEEC and FEM T-A based formulations

Laurea Magistrale in Mathematical Engineering - Ingegneria Matematica,

Author: Alessio Simoni

Advisor: Prof. Carlo De Falco

Co-advisor: Dr. Bernardo Bordini

Academic year: 2024-2025

---

1. Introduction

This thesis presents the modeling and testing of rare-earth barium copper oxide (REBCO) pancake coils for a 40 T Final Cooling Solenoid (FCS) of a Muon Collider [1], a proposed particle accelerator that collides muon beams for High Energy Physics purposes.

The magnet concept is based on a stack of non-insulated (NI) High Temperature Superconductor(HTS) [3] coils that must carry very high engineering current densities (exceeding 600 A/mm^2) in a compact geometry, represented in fig. 1.

Traditional mathematical formulations are accurate, but even with the inclusion of homogenization techniques, they are still extremely expensive when used on large, thin layered HTS coils for which the full 3D behavior is needed.

The presented efforts constitute a step in that direction, in parallel with others done at CERN using newly developed formulations [5].

The goal of this work has been to develop and validate the foundation of two 3D complete models for the transient simulation of superconducting magnets, connected to an extensive experimental program aimed at the realization of a 15 T sub-scale prototype before September 2026.

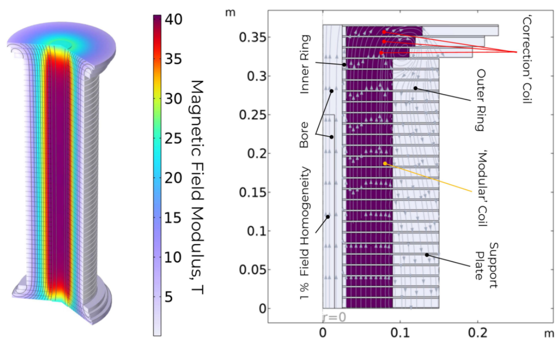

Figure 1: Layout and magnetic field distribution for the 40 T solenoid[1].

The research addresses this challenge by developing two separate tools. A 3D T–A [8] finite element method (FEM) model for spiral coils, the first of its kind for this geometry and application in COMSOL (see computational domain in fig. 2). A MATLAB partial element equivalent circuit (PEEC) integral model [6], using an innovative way to inject a transport current and a special quadrature rule for the weakly singular integral.

These two models, currently able to reproduce the behaviour of insulated coils, were benchmarked, and a first comparison between their predictions and the experimental data was performed.

2. Theoretical Foundation

In order to build numerical models that are more computationally efficient, it is useful to first reformulate the electromagnetic governing equations in terms of the T-A variables or in an integral form, suitable for FEM and PEEC implementation, respectively. Moreover, the specific problem allows for the use of the thin domain approximation, exploiting the strong aspect ratio of HTS tapes, additionally assuming that the represented current flow occurs only on the surface of the tape.

2.1. T–A formulation and thin-sheet approximation

The T–A formulation introduces the magnetic vector potential $\mathbf{A}$ and the current vector potential $\mathbf{T}$:

$$\mathbf{B} = \nabla \times \mathbf{A}, \qquad \mathbf{J} = \nabla \times \mathbf{T}.$$

Given $\Omega \subset \mathbb{R}^3$, the associated electromagnetic problem for a conductor domain $\Omega_c \subset \Omega$ in the magneto-quasistatic (MQS) regime reads:

$$\begin{cases} \nabla \times \left(\frac{1}{\mu_0} \nabla \times \mathbf{A} \right) = (\nabla \times \mathbf{T}), & \text{(1a)} \\ \mathbf{E} = \frac{\nabla \times \mathbf{T}}{\sigma(\mathbf{J}, \mathbf{B})}, & \text{(1b)} \\ \nabla \times \mathbf{E} = -\frac{\partial}{\partial t} (\nabla \times \mathbf{A}). & \text{(1c)} \end{cases}$$

Furthermore, the geometry of REBCO tapes, characterized by a 4 mm width and 80 μm thickness, is suitable for the use of the thin-sheet approximation. Therefore, the fields are modeled as uniformly distributed along the smaller dimension, and the current is assumed to flow on the surface of the tape.
In a local frame $\{\hat{\mathbf{r}}, \hat{\mathbf{t}}, \hat{\mathbf{z}}\}$ aligned with the radial, azimuthal, and axial directions, the current vector potential is reduced to

$$\mathbf{T} = [\mathrm{T}, 0, 0] = \mathrm{T}\hat{\mathbf{r}},$$

so for the electric vector potential the only unknown is a scalar field T.

2.2. PEEC integral equation

With the imposition of the Coulomb gauge, the uniquely defined magnetic vector potential can be expressed as a function of the current density, i.e., of the other unknown $\mathbf{T}$ by means of a weakly singular integral over the conductor.

$$\mathbf{A}(\mathbf{r}) = \frac{\mu_0}{4\pi} \int_{\Omega_c} \frac{\mathbf{J}(\mathbf{r}')}{|\mathbf{r} - \mathbf{r}'|} \, d\Omega_c + \mathbf{A}_0(\mathbf{r}). \qquad (2)$$

where $\mathbf{A}_0$ accounts for external sources.
The combination of (2) with Faraday's law gives an integral equation for $\mathbf{T}$:

$$\frac{\nabla \times \mathbf{T}}{\sigma} + \frac{\mu_0}{4\pi} \frac{\partial}{\partial t} \int_{\Omega_c} \frac{\nabla \times \mathbf{T}}{|\mathbf{r} - \mathbf{r}'|} \, d\Omega_c = -\frac{\partial \mathbf{A}_0}{\partial t}. \qquad (3)$$

This equation can be reinterpreted from a circuital point of view as Kirchhoff's law, with the left hand side being a resistive and inductive voltage drop, respectively.

3. Discretization and Quadrature

The COMSOL environment offered a high level interface for which the differential form of the equations and boundary conditions is sufficient for the implementation. On the other hand, the resolution of the PEEC equation in MATLAB required a detailed treatment of all the discretization aspects, such as the quadrature rules and the translation of a variational problem into an algebraic one through a standard Galerkin procedure. In this case, the external current injection was realized at this level, represented with the inclusion of an additional basis function, and the consequent extension of the finite dimensional form of $\mathbf{T}$.

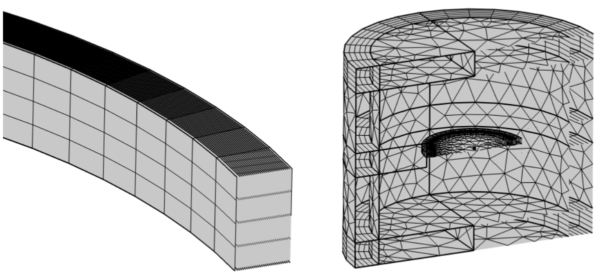

Figure 2: Mesh discretization of coil and air domain in COMSOL.

3.1. PEEC discretization and current injection

A standard Galerkin discretization was applied, and eq. (3) was discretized on Ω_c by means of $Q^1(K) = \{p(x, y) : \deg_x(p) \leq 1, \deg_y(p) \leq 1\}$ shape functions on rectangular mesh elements. This choice was made as the basis functions can be expressed analytically in the physical domain, eliminating the need for a reference domain and a mapping between the two, which significantly simplifies the implementation complexity.
Hence, T is computed over the mesh $\mathcal{T}_h$, in the finite dimensional functional space $V_h = \{v_h \in C^0(\Omega_c) : v_h|_K \in Q^1(K), \forall K \in \mathcal{T}_h\}$. Moreover, to address the more interesting excitation scenario of an external current I_0 being injected, an extra degree of freedom T_{N+1} and a lifting function $\mathbf{w}_{N+1}$ are introduced, so that T is discretized as:

$$\mathrm{T}_h = \sum_{k=1}^{N} T_k \mathbf{w}_k + T_{N+1}\mathbf{w}_{N+1}$$

with $\{w_i\}_{i=1}^N$ forming a basis of V_h with $N = \dim(V_h)$. For simplicity, $\mathbf{w}_{N+1}$ is designed to satisfy $\nabla \times \mathbf{w}_{N+1}\big|_{\partial\Omega} = \mathbf{J}_0/T_{N+1}$, correspond to a uniform imposed current density $\mathbf{J}_0 = \mathrm{I}_0/\mathrm{S}$ through the tape cross-section S.
The resulting algebraic system has the form

$$\mathbf{RT}(t) + \mathbf{L}\frac{\partial \mathbf{T}(t)}{\partial t} = \mathbf{b}(t), \tag{4}$$

where the resistance matrix $\mathbf{R}$ is sparse while the inductance matrix $\mathbf{L}$ is full, and b represents the forcing contribution.

3.2. Quadrature and time integration

The entries of $\mathbf{R}$ and $\mathbf{L}$ are integrals of the basis functions and their curls. Regular integrals were computed using Gauss-Legendre(GL) quadrature, while for self-inductance contributions, containing a weak singularity $1/|\mathbf{r} - \mathbf{r}'|$, a generalized Duffy transformation was used [4].
In the case of harmonic excitation scenarios and linear electric behaviour of the material, the frequency domain form of (4) can be used to eliminate the need for time stepping schemes, solving directly the associated stationary problem:

$$(\mathbf{R} + j\omega\mathbf{L})\mathbf{T}_f = \mathbf{f} \tag{5}$$

for the angular frequency ω associated with the external forcing.
For generic time-domain simulations, an implicit Backward Euler scheme was used due to his unconditional absolute stability, and at each time step, the solution of a linear system has to be performed.

3.3. 3D T–A FEM model

A 3D model is built in COMSOL using the same T–A formulation. The analyzed configurations are spiral geometries with 9 or 24 turns, surrounded by air.
The magnetic equation (1a) is solved with the *Magnetic Field Currents Only (mfco)* module of COMSOL, using quadratic edge elements for the computation of $\mathbf{A}$; while equation (1c) is implemented and solved with the *General Form PDE* module using linear nodal elements for T.

Turns	T–A FEM	PEEC
9	570 689	4 325
24	925 271	11 525
50	1 539 455	24 005

Table 1: Number of degrees of freedom (DoF) for the COMSOL T–A FEM and MATLAB PEEC models for coils with different numbers of turns.

4. Experimental Work

Several important milestones were pursued while aiming at enabling the construction of a 15 T subscale HTS solenoid, an intermediate step in the FCS project, towards the final 40 T objective. The major achievements were the optimization of a consistent, high quality, reproducible fully soldered REBCO pancake coil production process, the successful characterization of the electromagnetic behavior of single coils in terms of contact resistance between the layers and charging time constant, and the generation of benchmarking data for numerical models.

4.1. Testing setup and experiments

Tests were performed in liquid nitrogen at 77 K in self-field. The setup consists of a cryostat where the coil is fully immersed, copper current leads to inject and extract the current, two Hall probes and seven voltage taps to measure the magnetic flux density and the voltage distribution across the coil, respectively.
The current was supplied by a Delta Elektronika

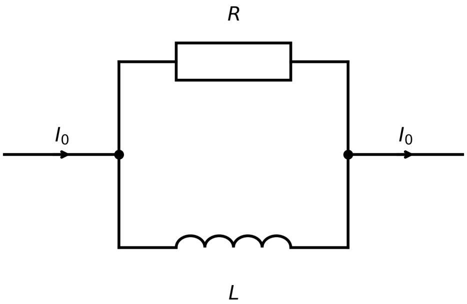

Figure 3: Equivalent circuit of an NI superconducting coil.

SM 30-200 DC power supply; voltages and Hall-probe signals were acquired with ten Keithley 2001 Digital Multi Meters having a resolution of $O(10^{-6})$ V.
Macroscopically, the superconducting coil can be very well approximated by a simple circuit having a resistance R in parallel with an inductance L, representing the radial and azimuthal electrical effects, respectively.
To determine these two main parameters, and obtain the charging time constant $\tau = L/R$, two sets of experiments were performed: current ramps at fixed rates (0.5 A/min) and current steps (5–20 A) in the range 0-150 A.
Moreover, the critical current of the coil I_c can be obtained. This is macroscopically defined as the maximum current before an energy dissipation (hence, a resistance and a voltage) over a certain threshold appears. For our experiments, it was defined in line with the standard 1μV/cm criterion for single samples [7], quantified on the length of the very first few inner turns, as they experience the critical state first, giving a reference voltage of (100–120 μV).

4.2. Main experimental results

When ramping below the critical current I_c, the measured voltage is dominated by the inductive behavior, however, a resistive component is also present due to the radial current flow. As the critical current I_c is approached, an additional linear resistive component appears, and the transitions can be sharp or broad depending on the quality of the fabrication process. For most coils, I_c at 77 K is consistent with the tape specifications when the self-field is taken into account.
The measured data provided a value of radial resistance R in the range of 20-35 $\mu\Omega$, an inductance L $\simeq$ 8 mH, and a time constant of 250–350 s.
In addition, the voltage and magnetic flux density evolution was monitored as a function of the injected current to establish the performance of the fabricated superconducting pancake coils.
In particular, for the voltage measurements, the coil was instrumented to be split into 6 circular concentric but distinct sectors, as the voltage taps were positioned radially. In the case of a current steps experiment, the obtained voltage distribution in the different regions of the coil is represented in fig. 4. In a final experiment, a coil

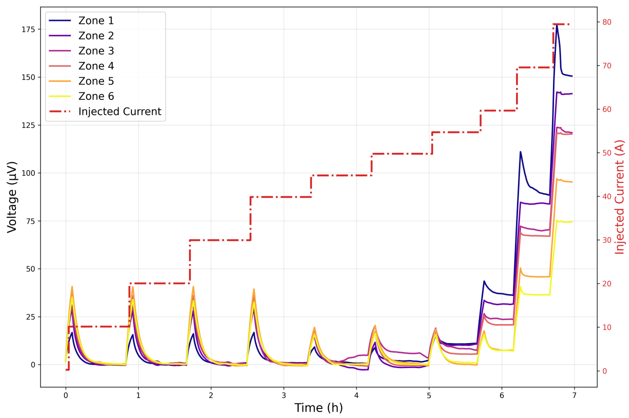

Figure 4: Measured voltage in different sectors of the coil, from the innermost (Zone 1) to the outermost (Zone 6).

was polished. For this test, the copper stabilizer, as well as the solder on both flat faces of a coil, was removed by mechanical polishing. This was done to suppress the normal conducting path between turns, exploiting the isolating properties of the buffer layers, embedded in the architecture of the coated conductor. Hence, in first approximation, the equivalent circuit of such a coil is constituted only by an inductor, as the radial resistance has become two orders of magnitude larger than before. As a consequence, the time constant dropped from about 320 s to just 2 s while the linear B–I dependence below I_c remained unchanged. Therefore, it is reasonable to assume that the damage to the superconducting layer was negligible. However, the coil now behaves effectively as insulated.

5. Validation

The PEEC implementation was first tested on a rectangular strip($L_x = L_z = 0.1$ m, $\delta = 3$ mm, $\sigma \approx 4.7 \times 10^6$ S/m) and benchmarked in the frequency domain against a PEEC Octave and COMSOL A-V models, for a uniform applied field and an imposed current $I_0 = 30$ A, respectively. It is worth underlining that the frequency range of interest for magnet applications is 0.1-10^2 Hz.

Current density distributions and Joule losses were compared. The agreement is within a few percent from 1 Hz up to 10 kHz, progressively increasing as the thin domain assumptions break down for higher frequencies.

Before moving to the transient simulation of spiral domains, the time stepping scheme was validated against the frequency domain resolution, in a scenario with harmonic forcing. A Fourier transform analysis shows that the Backward Euler time-domain solution converged to the frequency-domain steady-state one in both amplitude and phase.

The behavior of 9, 24 and 50-turn spirals was analyzed and tested on the same experimental current ramps. The MATLAB PEEC and 3D COMSOL T–A models match on the local eddy currents in the winding, the evolution of the total Joule losses, and of the magnetic flux density at the center and on-coil as shown in fig. 5.

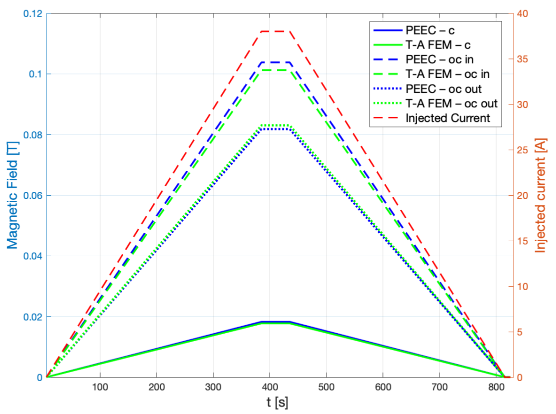

Figure 5: Magnetic flux density comparison for a 24-turn coil in the center (c) and on coil (oc) on the innermost (in) and outermost (out) turn.

The maximum relative discrepancies are around 0.1-1% for current density and Joule losses, and 2–3% for the magnetic flux density during the ramp and in steady state. This shows that the thin-sheet PEEC approximation, with the new current injection method, can reproduce the 3D response of realistic spiral coils with far fewer degrees of freedom (see table 1).

6. Model–Experiment Link

The 3D COMSOL T–A model is also suitable for the simulation of the complete non-linear behaviour of an insulated REBCO coil, as the one mentioned in section 4.2. A power-law E–J relation is used,

$$\mathbf{E} = E_0 \left(\frac{\mathbf{J}}{J_c} \right)^n ,$$

with $E_0 = 100\,\mu\text{V/m}$, $J_c(B,T)$ critical current density, taken from manufacturer data, and n typically being 20-40. The trend of the center field, as the number of turns is increased, tends to the distribution that was experimentally measured in the polished coil (see fig. 6). The dependence of the magnetic flux density from the injected current remains linear, but once the critical current is reached, the coil quenches, i.e., loses its superconducting state. The computational effort required for the simulation is the only limitation towards the direct simulation of a full scale coil. This issue is going to be tackled by means of memory and assembling optimization strategies as the use of Hierarchical Matrices or the Fast Multipole Method [2].

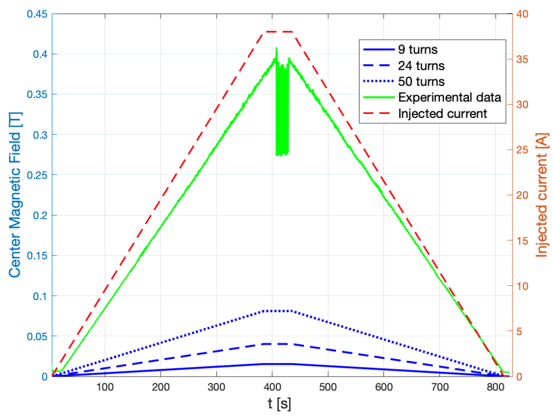

Figure 6: Indirect comparison between numerical (in blue) and experimental (in green) results for an insulated coil.

The last necessary step to tackle NI REBCO coils is to include the radial flow of the current.

7. Conclusions

The thesis has developed and validated a PEEC integral model in MATLAB for thin rectangular and spiral conductors with linear resistivity, using a new current injection strategy; and a 3D T–A FEM model in COMSOL for superconducting insulated coils.

The two numerical models agree within a few percent on eddy currents, Joule losses and magnetic field densities for both 9, 24 and 50-turn spirals. The thin-sheet PEEC formulation reproduces the 3D T–A results with far fewer unknowns. In addition, the current results show a very promising consistency with the experimental data for the magnetic field generated in the center of an HTS insulated coil.

Experimentally, more than twenty NI REBCO pancakes were fabricated and tested at 77 K to measure their electrical properties and explore their performance, representing an early but important step in the plan towards a 40 T for a Muon Collider and providing useful data to benchmark the numerical models.

8. Future Developments

The very next steps constitute the natural prosecution along the path towards a complete numerical simulation of NI REBCO coils and the assembly and testing of a 15 T peak field solenoid. From the numerical point of view, the main focus is going to be on completing the implementation of the nonlinear power-law behaviour in the PEEC model and benchmarking it against the COMSOL T–A model, to then extend both models to include radial current paths and NI behaviour. On the other hand, the next experimental goals are also very clear. In fact, a setup to test single and double pancakes at 4.2 K is already under development, together with the design of different possible ways to electrically joint multiple coils, in order to realize a proper solenoid. Later on, a testing campaign at 4.2 K and in background fields up to about 20 T is foreseen to operate the magnet under realistic operational conditions.

Overall, the first results at 77 K of the past months are very promising signs towards a subscale solenoid prototype. Once the performance is confirmed also at 4.2 K and for a stack of 14 coils, the feasibility of the main critical component of a Muon Collider will be one step closer to its realization.

9. Bibliography

References

[1] B. Bordini, C. Accettura, A. Bertarelli, L. Bottura, A. Dudarev, A. Kolehmainen, T. Mulder, A. Verweij, and M. Wozniak. Conceptual design of a rebco non/metal-insulated ultra-high field solenoid for the muon collider. *IEEE Transactions on Applied Superconductivity*, 34(3):1–10, May 2024.

[2] P. Rapp M. Bebendorf L. Gaul D. Brunner, M. Junge. Comparison of the fast multipole method with hierarchical matrices for the helmholtz-bem. *Computer Modeling in Engineering & Sciences*, 58(2):131–160, 2010.

[3] Beate R. Lehndorff. *High-Tc Superconductors for Magnet and Energy Technology*. Springer Berlin Heidelberg, December 2000.

[4] S. E. Mousavi and N. Sukumar. Generalized duffy transformation for integrating vertex singularities. *Computational Mechanics*, 45(2–3):127–140, October 2009.

[5] Davide Rinaldoni. Multiscale numerical modelling of non-insulated rebco superconducting coils. Master's thesis, Politecnico di Milano, https://hdl.handle.net/10589/223554, 2023/2024.

[6] Jonathan Siau. *Unstructured PEEC formulationsconsidering resistive, inductiveand capacitive effects forpower electronics*. Theses, Université Grenoble Alpes, December 2016.

[7] Victor M. R. Zermeño, Frederic Sirois, Makoto Takayasu, Michal Vojenčiak, Anna Kario, and Francesco Grilli. A self-consistent model for estimating the critical current of superconducting devices. *Superconductor Science and Technology*, 28(8):085004, June 2014.

[8] Huiming Zhang, Min Zhang, and Weijia Yuan. An efficient 3d finite element method model based on the t–a formulation for superconducting coated conductors. *Superconductor Science and Technology*, 30(2):024005, December 2016.